Role of Molecular Anchor Groups in Molecule-to-Semiconductor Electron Transfer†

Ralph Ernstorfer,*,‡,|| Lars Gundlach,‡ Silke Felber,‡ Winfried Storck,§ Rainer Eichberger,‡ and Frank Willig*,‡

Dynamics of Interfacial Reactions SE 4, Hahn-Meitner-Institut, Glienicker Strasse 100, D-14109 Berlin, Germany, and Fritz-Haber-Institut der Max-Planck-Gesellschaft, Faradayweg 4-6, 14195 Berlin, Germany

Received: July 13, 2006; In Final Form: August 30, 2006

The dynamics of heterogeneous electron transfer (ET) from the polycyclic aromatic chromophore perylene to nanostructured TiO_2 anatase was investigated for two different anchor groups with transient absorption spectroscopy in an ultrahigh vacuum. Data from ultraviolet photoelectron spectroscopy and from linear absorption spectroscopy showed that the donor state of the chromophore was located around 900 meV above the lower edge of the conduction band. With the wide band limit fulfilled the rate of the heterogeneous ET reaction was only controlled by the strength of the electronic coupling and not reduced by Franck−Condon factors. Two different time constants for the electron transfer, i.e., 13 and 28 fs, were measured with carboxylic acid and phosphonic acid as the respective anchor groups. The difference in the ET time constants was explained with the different extension of the donor orbital onto the respective anchor group to reach the empty electronic states of the semiconductor. The time constants were extracted by means of a simple rate equation model. The validity of applying this model on this ultrafast time scale was verified by comparing the rate equation model with an optical Bloch equation model.

I. Introduction

The injection of electrons from a molecular adsorption layer into a semiconductor via absorption of visible light has been established already with the invention of dye-sensitized AgBr photography[1] more than a century ago. More recently, the same basic process has been successfully utilized for efficient photovoltaic energy conversion in dye-sensitized solar cells.[2] Scenarios for molecular devices in the proposed field of molecular electronics[3] require at some point the transfer of electrons from molecular moieties to an electrode. Heterogeneous electron transfer (HET) from an electronic excited molecular donor to a solid electrode represents a unique electron-transfer (ET) case if the donor level is energetically positioned high enough so that a wide continuum of empty electronic states of the electrode can be utilized as acceptor states. One refers to this situation as the wide band limit, where all the Franck−Condon factors of the ET reaction are available in parallel.[4] In the wide band limit the ET rate is only controlled by the strength of the electronic coupling between the donor orbital and the electronic acceptor states and by the density of states (DOS) at the surface of the electrode.[5−9] In recent years, the kinetics of HET has been studied for numerous organic and metal−organic sensitizers on different oxide semiconductors and in different environments. A wide spread of time constants for electron injection ranging from sub-10-fs to hundreds of picoseconds has been reported.[10−21] This wide range of time constants can be traced back in many cases to a key parameter of the HET reaction, which is the strength of the electronic coupling between the molecular donor state and the acceptor states, where the latter can be both bulk and surface states, as the electronic structure on the surface of the semiconductor is highly sensitive to details of the atomic structure. After the electron is transferred to electronic states of the solid, the specific band structure and the specific electron−phonon coupling have a strong influence on the dynamics of the hot electrons.[22−24] To reach a microscopic understanding of the interfacial electron-transfer process, the nature, in particular the (de-)localization, of the photoexcited state on the adsorbed chromophore has to be known. It is obvious that with increasing electronic interaction the molecular electronic structure and the semiconductor states cannot be assigned to separate states any longer since the eigenstates of the system gradually become mixed states that are delocalized over both adsorbate and solid. A specific example for a strongly interacting molecular adsorbate is catechol adsorbed to TiO_2, where catechol is known to form a surface chelate. Such a surface complex can give rise to a direct optical charge-transfer band, where the corresponding photoinduced charge transfer is not HET but a completely different process, i.e., internal photoionization.[25−28] A great variety of different light-absorbing chromophores has been employed already in various studies of photoinduced HET, e.g., the well-known cyanine dyes and their derivatives,[29] xanthene dye molecules such as rhodamine B and cresyl violet,[12] aromatic molecules such as perylene,[10,30] metal−organic compounds such as Ru−bipirydyl and various derivatives,[2,13] and finally also inorganic compounds[31,32] such as $[Fe(CN)_6]^{4-}$. For most of the device applications a slow recombination reaction is desired for the hole that is generated via electron injection in the form of the ionized chromophore, of course combined with a fast injection process.

Inserting an anchor group between the actual chromophore and the surface of the semiconductor helps in at least three ways.

† Part of the special issue "Arthur J. Nozik Festschrift".

* Authors to whom correspondence should be addressed. E-mail: ralph@lphys.chem.utoronto.ca; willig@hmi.de

‡ Hahn-Meitner-Institut.

§ Fritz-Haber-Institut der Max-Planck-Gesellschaft.

|| Present address: Department of Chemistry, 80 St. George St., University of Toronto, Toronto, ON M5S 3H6, Canada.

10.1021/jp064436y CCC: $33.50
Published on Web 10/20/2006

First, it can provide a better-defined adsorption geometry with a stronger surface bond than is usually achieved by directly depositing the unmodified chromophore on the surface of the solid. This first point had been realized already several decades ago for such interfacial electron-transfer systems.[33] Later such acid groups have been mostly employed as the anchor groups for attaching chromophores to the surfaces of oxide electrodes such as TiO_2. Strong adsorption bonds formed by such anchor groups can lead to a well-defined adsorption geometry at the interface that is preserved up to temperatures well above room temperature. This has been confirmed recently by angle- and polarization-dependent two-photon photoemission signals measured on the rutile TiO_2(110) surface for the perylene chromophore with different anchor/bridge groups.[34] Second, a suitable anchor group can slow recombination. Third, a suitable anchor group can keep the molecular orbital essentially localized on the chromophore part of the adsorbed molecule. It will be shown here that the insertion of acids as anchor groups is still compatible with electron injection times in the range from a few femtoseconds to several tens of femtoseconds. This keeps HET faster than any other decay process for the excited molecular donor state.

Two different anchor groups, i.e., $-$COOH and $-PO_3H_2$, were investigated in this work. The perylene chromophore was adsorbed with the respective anchor group at the inner walls of nanometer-size cavities formed in a colloidal layer of anatase TiO_2. This nanometer-structured layer was developed earlier by Grätzel and co-workers for the electrochemical dye-sensitized solar cell.[35] These authors have shown that the (101) face of anatase TiO_2 dominates the inner surface of the nanometer cavities in the colloidal layer of anatase TiO_2. The surface of TiO_2 is sufficiently robust such that the acid groups can form strong bonds to Ti atoms on the surface without dissolving the crystal lattice and release of the corresponding salt into the adjacent solution phase. The latter effect has been shown to occur with ZnO whose lattice is known to be less robust.[21]

It has remained a long-standing question concerning HET to what extent certain electron-transfer parameters, foremost the electron-transfer time, are affected by the insertion of an anchor group, or more generally an anchor/bridge group, between the actual chromophore and the semiconductor. We present here to our knowledge the first time-resolved data on electron transfer for the same specific aromatic chromophore, here perylene, when the latter is bonded with two different acid groups, i.e., $-$COOH and $-PO_3H_2$, to the surface of a semiconductor, here TiO_2. Transient absorption measurements (pump$-$probe) were carried out with sufficient time resolution (cross-correlation function shorter than 30 fs full width at half-maximum (fwhm)) in an ultrahigh vaccuum (UHV) where the rise of the ionized state of the chromophore perylene was monitored in response to an ultrashort laser pulse. The measured time-dependent rise probes directly the time-dependent release of the electron from the first excited singlet state of perylene into the empty electronic states of TiO_2.[10,36] With perylene as the chromophore there are no fast intramolecular dynamics competing with electron transfer. Such competing processes have been shown to be significant in, for example, the Ru dyes, where fast intersystem crossing[13] and fast interligand transfer/localization[37] have a pronounced influence on the injection kinetics. The dominant decay channel of the excited state of the isolated perylene is via fluorescence with a time constant of approximately 5 ns. Thus, electron transfer is the only efficient decay channel for the photoexcited state of the adsorbed molecule.[38] The electronic structure of the interface was studied with photoelectron spectroscopy, and we report here that the donor level of perylene lies high enough to fulfill the wide band limit. The transient absorption measurements revealed electron-transfer times of 13 and 28 fs for the two different anchor groups. Our interpretation of the effect of the two different anchor groups on the electron-transfer time was inspired by quantum chemical calculations for the molecules in the gas phase. From recent structure calculations[39] it can be inferred that both the orientation of the perylene chromophore and also the distance of the aromatic ring system of the perylene chromophore from the (101) surface of anatase TiO_2 are rather similar for these two different anchor groups. The adsorption geometry predicted in the above reference has been confirmed by recent measurements performed for the perylene chromophore with different anchor/bridge groups on the (110) surface of rutile.[34] The quantum chemical calculations for the isolated molecules showed that the spatial extension of the chromophore's donor orbital into the respective anchor group is very different. Recent density functional theory (DFT) cluster calculations have confirmed the same qualitative trend for the lowest unoccupied molecular orbital (LUMO) state of the perylene chromphore when adsorbed with different anchor/bridge groups on a large TiO_2 cluster.[40] Thus, the difference in the measured electron-transfer times was ascribed to the difference in the strength of the respective electronic coupling. The latter is a measure for the extension of the donor orbital onto the respective anchor group to reach the empty states of the semiconductor.

II. Experimental Section

For this work two different perylene derivatives were synthesized, each contained perylene with three covalently attached side groups. The bond with the semiconductor was formed by an anchor group, which was either the carboxylic or the phosphonic acid group (in the 9-position). Two bulky groups (*tert*-butyl) in the 2- and 5-positions prevented dimerization of neighboring perylene chromophores when attached to the surface of TiO_2. A detailed description of the synthesis of (2,5-di-*tert*-butyl-perylen-9-yl)carboxylic acid (DTB$-$Pe$-$COOH) and (2,5-di-*tert*-butyl-perylen-9-yl)phosphonic acid (DTB$-$Pe$-PO_3H_2$) is given in the Supporting Information.

Nanostructured anatase films with a thickness of approximately 2 μm were used as the transparent semiconductor functioning as an electron acceptor in the photoreaction. The preparation of the nanoparticles and of the nanostructured films formed from these particles followed procedures described by Grätzel et al.[41] Transmission electron microscopy (TEM),[42] X-ray diffraction (XRD) measurements, and Raman spectroscopy indicate the anatase phase of TiO_2. The size distribution of the colloids peaks at approximately 15 nm diameter; the dominating surface is the (101) face.[35] The colloidal films were deposited on a glass substrate using a film applicator (Erichsen, Coatmaster 509MC). Brunauer$-$Emmett$-$Teller (BET) measurements of these films indicate a surface area of approximately 140 m^2/g and a mean pore diameter of 9.5 nm. To minimize coherent contributions to the pump$-$probe signal from the glass substrate, approximately 50-μm-thick glass sheets (Schott, glass type AF45) were used for the transient absorption measurements, whereas the ultraviolet photoelectron spectroscopy (UPS) and X-ray photoelectron spectroscopy (XPS) measurements were performed on samples with conducting substrate (500 nm SnO_2:F on 1 mm float glass). Prior to adsorption of the dye, the TiO_2 films were brought to 450 °C for 45 min in laboratory ambient. The films were coated with the dye by immersing them into a dye solution (10^{-4} M in toluene) at room temperature

for 5−10 min (DTB−Pe−COOH) and 20−25 min (DTB−Pe−PO_3H_2), both resulting in an absorbance of 0.5−0.8 OD at 450 nm. Linear absorption spectra were recorded with Bruins Instruments Omega 10 and 20 UV−vis−near-IR spectrometers. Samples for XPS/UPS measurements were colored to an absorbance of 1.0−1.2 OD. Both treatments did not saturate the binding sites in the anatase film. The dye-covered TiO_2 electrode was rinsed with dried solvent, blown off with argon, and then quickly transferred via a load-lock chamber into an UHV chamber with a base pressure in the 10^{-10} mbar range. A detailed description of the UHV chamber is given elsewhere.[43] Besides some initial drop in signal strength, the samples were found to be stable for hours during the pump−probe measurements under UHV conditions. This behavior in a vacuum was rather different from the gradual degradation of otherwise identical systems if exposed to the laboratory ambient. It is known, for example, that water is reacting with the cationic state of perylene, thereby splitting the aromatic ring system.[44] Also the stability during storage under UHV conditions of the samples is clearly improved as no degradation could be observed over some months.

Stationary photoemission spectra were recorded normal to the surface with a hemispherical analyzer (VSW HAS 100) in a separate UHV chamber. A commercial X-ray source (Mg Kα) and a He UV discharge lamp ($h\nu$ =21.22 eV) were used for excitation. Due to the limited conductivity of the nanostructured anatase films, charging of the samples during XPS/UPS measurements is a problem at room temperature. This can be overcome by moderately heating the samples as the conductivity of nanostructured anatase is strongly temperature-dependent.[45] Heating the samples to approximately 370 K, which is below the desorption and the decomposition temperatures of the adsorbates, turned out to be sufficient for preventing charging of the 2-μm-thick films during the measurements.

Laser pulses for transient absorption measurements were generated with a 100 kHz repetition rate Ti:sapphire laser system (Coherent Instruments; seed, Mira 900; amplifier, RegA 9050) operating at 800 nm. The oscillator and amplifier were pumped by two solid-state lasers (Coherent 5 and 10 W Verdi). The laser system provided pulses of 7 μJ energy and 50 fs pulse duration fwhm. Pump pulses in the range of 420−450 nm were generated from 85% of the pulse energy by use of a noncollinear optical parametric amplifier (NOPA),[46] which was designed for low pulse energies.[47,48] The NOPA provided broadband near-infrared (NIR) output centered at 870 nm, which was frequency-doubled in a 100-μm-thick β-barium borate (BBO) crystal, resulting in Gaussian-like spectra centered at 435 nm with 25 nm fwhm. Compression of the blue pulses was achieved by precompensation, i.e., down-chirping, of the NIR pulses in a standard fused silica prism compressor. The autocorrelation function measured with a home-built intensity autocorrelator (type I second harmonic generation in a 50 μm BBO crystal or two-photon photocurrent in a SiC diode) indicated pulse durations below 15 fs fwhm. The energy of the pump pulses at the sample was 15 nJ or less. Weak probe pulses of approximately 0.3 nJ in the spectral range of the perylene cation absorption at approximately 570 nm were filtered from a white light continuum generated by 15% of the 800 nm pulses in a 1-mm-thick sapphire plate. Compression was realized by a prism compressor (BK7 glass). Pump and probe pulses were moderately focused to spot diameters of approximately 150 and 100 μm, respectively, under an angle of 2°. The polarizations of pump and probe pulses were kept parallel as the pumped (ground-state absorption) and the probed (cationic ground-state absorption) electronic transitions exhibit the same symmetry.[49] The instrumental response function of the setup was obtained outside the UHV chamber as the two-photon photocurrent absorption signal in a windowless SiC photodiode (Laser Components), which has been shown to give very reliable cross-correlations.[50] Pulse intensity, pulse duration, and beam profile showed good stability during the experiment. The cross-correlations taken before and after the transient absorption measurements were in the range of 27 ± 1 fs (fwhm). Further experimental details were qualitatively identical with those described elsewhere.[9,10,17] All experiments except UPS were performed at room temperature.

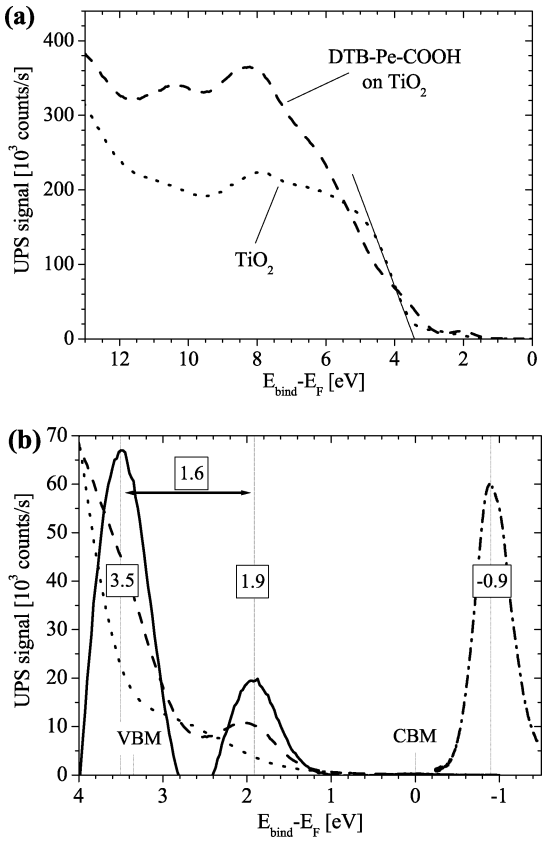

Figure 1. He−I spectra of sensitized (dashed line; dye, DTB−Pe−COOH) and unsensitized nanostructured anatase films (dotted line). (b) Range around the band gap. The difference spectrum (solid line, enlarged by a factor or 3) shows the HOMO at 1.9 eV binding energy and the HOMO − 1 and HOMO − 4 states around 1.6 eV lower in energy. The position of the molecular excited state, i.e., the donor of the electron injection process, is estimated by adding the photon energy at the onset of the absorption spectrum to the energy −1.9 eV at the center of the HOMO peak (dash−dotted line).

Molecular orbital (MO) calculations were performed with HyperChem, release 7.03, Hypercube, Inc., with the PM3 parametrization, a semiempirical self-consistent-field procedure. The molecular geometries were optimized with the Polak−Ribiere algorithm and terminated when the gradient became less than 0.001 kcal/(Å mol).

III. Results

A. Energy Level Alignment at the Interface. With respect to the ET reaction, the energetic position of the molecular donor state relative to the empty electronic states of the semiconductor is an important property of the interface as it determines the available energy range and density of acceptor states.

Figure 1 shows He−I UPS spectra of sensitized (dashed line; dye: DTB−Pe−COOH) and unsensitized (dotted line) nano-

structured anatase films. The spectrum of the unsensitized film exhibits the O 2p valence band[51] with binding energies (E_{bind}) in the range of 3.3−9 eV below the Fermi energy (E_F), similar to the valence band of anatase single crystals,[52,53] followed by the onset of an intense secondary electron signal toward higher binding energies (Figure 1a). The position of the valence band maximum (VBM) was determined at 3.4 eV below E_F by a linear fit of the falling edge from the unsensitized film taking into account the energy resolution of the setup. A fit of the onset of the optical absorption[54] according to $\sqrt{\alpha(E)E} = \alpha_0(E - E_{gap})$ reveals an optical gap of 3.35 eV, which implies that E_F is very close to the conduction band minimum (CBM) under measuring conditions.

The difference spectrum of the dye-loaded and the pure anatase films (solid line in Figure 1b) exhibits two peaks separated by 1.6 eV in the region of the band gap. These peaks are in good agreement with UPS data of perylene in the gas phase[55] and can be assigned to the highest occupied molecular orbitals (HOMOs) of the core chromophore. The DOS's of both dyes provide a similar spectrum: According to semiempirical calculations (ZINDO/S on PM3-optimized geometries), the molecular peak at 1.9 eV binding energy arises from the HOMO only, whereas four close lying states (HOMO − 1 to HOMO − 4) contribute to the peak at 3.5 eV binding energy in the UPS difference spectra. The position of the molecular excited state can be estimated by adding the optical excitation energy to the position of the HOMO. The corresponding peak is shown as a black dash−dotted line at negative binding energies in Figure 1b, which is not UPS data but rather the absorption spectrum of the adsorbed dye relative to the HOMO maximum at 1.9 eV binding energy. This spectrum peaks 900 meV above E_F ($\sim E_{CBM}$). The vibrational ground state is approximately 150 meV lower in energy. Thus, the spectrum at negative energies in Figure 1b gives a good idea of the relative position of the donor orbital with respect to the conduction band levels of TiO_2.

There should be two remarks with respect to the above estimation of the energetic position of the excited state. First, it is assumed that the position of the HOMO is at the maximum of the peak at 1.9 eV binding energy. However, it is plausible that this peak is the inhomogeneously broadened Franck−Condon progression of the photoemission process (cf. gas-phase data[55]), implying that the position of the HOMO and hence the position of the excited state is somewhat higher in energy. Second, adsorption of the dye might induce a dipole layer at the interface,[56,57] which also affects the relative position of the molecular states. For instance, for a metal−organic dye adsorbed on TiO_2, a surface dipole of 0.2 eV has been identified by a shift of the substrate core levels upon adsorption of the dye.[58] For the perylene chromophores studied in this work such a shift is not observed in XPS measurements. The adsorption of the chromophore only reduces the intensity of the substrate core level peaks Ti 2p and O 1s, but neither the positions nor shapes of the peaks are altered due to the adsorption of the chromophore. The peak positions obtained from fits of the XPS data are 459.37/459.39 eV (without/with adsorbate) for the Ti $2p_{3/2}$ and 530.71/530.72 eV for the O 1s levels. This might indicate that the surface dipole in the perylene/anatase system is weaker than that in the Ru−dye/anatase system studied in ref 58.

Identical UPS and XPS measurements were performed for DTB−Pe−PO_3H_2-sensitized anatase films. The HOMO as well as the C 1s core level peaks of this dye tend to be slightly ($\sim$50 meV) lower in binding energy compared to those of DTB−Pe−COOH; however, such small shifts are close to the detection limit. It is important to note that the difference in the position of the excited state of both perylene dyes is much smaller than the distance of the donor levels from the CBM, and hence the available density of acceptor states for the ET reaction is very similar for both adsorbates.

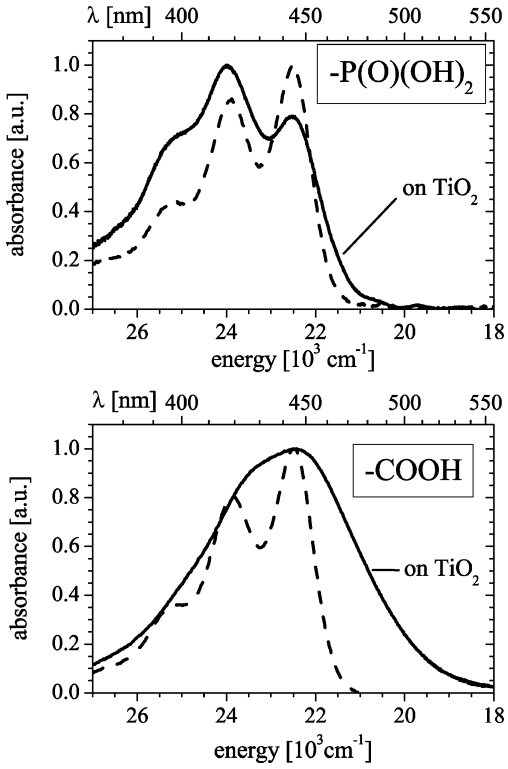

Figure 2. Dye absorption spectra of DTB−Pe−PO_3H_2 (upper panel) and DTB−Pe−COOH (lower panel). Solid lines represent the normalized net dye absorption of the adsorbed chromophores, i.e., the difference spectra of sensitized and unsensitized TiO_2 films. Dashed lines represent normalized absorption of the free dyes in 1:1 toluene/methanol.

B. Absorption Spectra. Figure 2 shows the absorption spectra of DTB−Pe−COOH and DTB−Pe−PH_2O_3 in solution (toluene/methanol 1:1, dashed lines) in comparison with the absorption spectra of the same molecules adsorbed on TiO_2 (laboratory air, solid lines). In solution, both dyes show a very similar absorption spectrum for wavelengths longer than 370 nm, which corresponds to the characteristic Franck−Condon progression of the $S_0(A_g) \rightarrow S_1(B_{1u})$ transition of perylene.[49,59] However, the absorption spectra of the dyes attached to the semiconductor were significantly different: In the case of DTB−Pe−COOH, the Franck−Condon progression of the net dye absorption (solid line) in the sensitized film was almost washed out, the absorption band was significantly broadened with a tail on the red edge of the absorption band, and the whole band appeared to be slightly red-shifted. In the case of the phosphonic acid anchor, the spectral changes due to the adsorption were significantly weaker: The Franck−Condon structure was preserved without spectral shift but showed different relative intensities, and there was only a weak red tail compared to the spectrum of this dye in solution.

C. Electron-Transfer Dynamics. Injection of electrons from a different perylene chromophore into nanostructured TiO_2 anatase film has been time-resolved previously by measuring transient absorption signals of the perylene chromophore: first the decay of the excited singlet state at 715 nm,[36,42] second the rise in the population of the ionized state by probing the perylene cationic $D_0 \rightarrow D_5$ transition[49,60] at 570 nm,[36,42] and third the

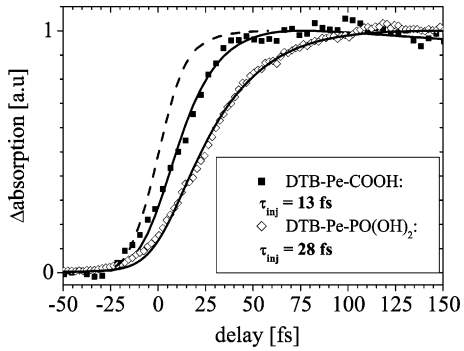

Figure 3. Transient absorption signals of DTB−Pe−COOH (squares) and DTB−Pe−PO_3H_2 (diamonds) measured at 565 nm after excitation with a sub-15-fs pump pulse centered at 435 nm. For a better comparison a signal offset before time zero has been subtracted, and the data have been normalized. Solid lines represent monoexponential fits of the data. The fit of the data according to eq 1 is given as a solid line and reveals time constants τ_{inj} of 13 and 28 fs. The integral of the measured cross-correlation is given as a dashed line.

rise in the population of the injected electrons measured as intraband transition at 1325 nm.[36] The three different signals gave the same monoexponential charge-transfer rate. As the strong $D_0 \rightarrow D_5$ transition of the perylene cation is spectrally well separated from the ground-state absorption, from the excited-state absorption, and from the emission of the neutral dye, the kinetics of its rise are directly accessible at a single probe wavelength. Figure 3 compares the rise of the cationic absorption signal for the two different anchor groups, taken as the transient absorption signal at 565 nm with a spectral resolution of 2 nm after excitation with a 15 fs (fwhm) pump pulse centered at 435 nm. There is some signal offset before the arrival of the pump pulse, which corresponds to some remaining perylene cation population from previous pump pulses (pulse separation 10 μs). For the sake of comparability, the offset is subtracted, and the data are normalized in Figure 3. Both dyes show significantly different kinetics. The simplest approach for the extraction of time constants from the pump−probe signals is the use of a rate equation model. The minimal rate equation model assumes the electron injection as a monoexponential decay (with a time constant τ_{inj}) of the photoexcited state into the cationic state, which itself decays monoexponentially ($\tau_{rec,i}$) due to recombination. The time dependence of the perylene cation population $N_{cat}(t)$ is then given by

$$N_{cat}(t) = N_0 \frac{\tau_{rec}}{\tau_{rec} - \tau_{inj}}(e^{-t/\tau_{rec}} - e^{-t/\tau_{inj}}) \qquad (1)$$

The fit of the experimental data with this approach, including the convolution with the experimental cross-correlation, reveals injection times of 13 and 28 fs for the perylene carbonic acid and phosphonic acid, respectively.

It should be noted that the interpretation of the above time constants as injection times assumes that the cationic absorption directly reflects the population of the cationic ground state. The intuitive definition of the electron injection kinetics is the decay of the projected charge density of the photoexcited state on the dye.[61] The transition probed in the experiment, the bright $D_0 \rightarrow D_5$ transition, has strong HOMO−LUMO character with contributions from both α and β electron spaces in an open shell description of the cation.[49] All four wave functions involved in the transition are delocalized over the perylene ring structure. Therefore, the cationic absorption can be assumed as a good measure of the cation population even on the ultrafast time scale.

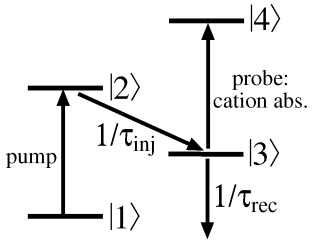

Figure 4. Schematic illustration of the four-level system modeled with the OBEs.

The rate equation model applied above only describes the populations in the relevant electronic states and neglects the field-induced polarizations between the states. Therefore, it is in general only applicable if the population transfer within the system is slow compared to the electronic dephasing time.[62] It is not clear whether this condition is fulfilled in the system investigated here. For this reason the pump−probe signals were fitted with optical Bloch equations (OBEs). A four-level scheme, as illustrated in Figure 4, was considered for the simulation of the pump−probe signals with the cationic absorption as the probe transition. The levels $|1\rangle$ and $|2\rangle$, ground and photoexcited states, are coupled by the pump field. The electron injection is described as an incoherent coupling of the photoexcited state to the cationic ground state $|3\rangle$. (The population relaxation time T_1 of the photoexcited state is thus τ_{inj}.) The probe field couples $|3\rangle$ and the cationic excited state $|4\rangle$. The model should be seen as two incoherently coupled two-level systems rather than a true four-level system as no polarizations between the neutral and the cationic moieties are allowed. Within the rotating wave and dipole approximations and with the restrictions to purely resonant transitions and weak electric fields, the OBEs read for the relevant components of the density matrix $\rho(t)$

$$\dot{\rho}_{22}(t) = \frac{\mu_{12}E_{pump}(t)}{2i\hbar}(\rho_{12}(t) - \rho_{21}(t)) - \frac{\rho_{22}(t)}{\tau_{inj}} \qquad (2)$$

$$\dot{\rho}_{12}(t) = \rho^*_{21}(t) = \frac{\mu_{12}E_{pump}(t)}{2i\hbar}(\rho_{22}(t) - \rho_{11}(t)) - \frac{\rho_{12}(t)}{T_2^{(1)}} \qquad (3)$$

$$\dot{\rho}_{33}(t) = -\frac{\mu_{34}E_{probe}(t - t_d)}{2i\hbar}(\rho_{34}(t) - \rho_{43}(t)) + \frac{\rho_{22}(t)}{\tau_{inj}} - \frac{\rho_{33}(t)}{\tau_{rec}} \qquad (4)$$

$$\dot{\rho}_{34}(t) = \frac{\mu_{34}E_{probe}(t - t_d)}{2i\hbar}(\rho_{44}(t) - \rho_{33}(t)) - \frac{\rho_{34}(t)}{T_2^{(2)}} \qquad (5)$$

$$\dot{\rho}_{44}(t) = \frac{\mu_{34}E_{probe}(t - t_d)}{2i\hbar}(\rho_{34}(t) - \rho_{43}(t)) \qquad (6)$$

$E_{pump}(t)$ and $E_{probe}(t - t_d)$ denote the envelopes of the electric fields of the (spectrally separated) pump and probe pulses. $T_2^{(1)} = (1/2\tau_{inj} + 1/T_2^{(1)*})^{-1}$ is the dephasing in the neutral molecule, where $T_2^{(1)*}$ represents the pure dephasing. The dephasing of the cationic states $T_2^{(2)}$ is assumed to be determined by the pure dephasing, i.e., $T_2^{(2)} = T_2^{(2)*}$.

The signal $I_{pp}(t_d)$ of the pump−probe experiment is the polarization $P^{(3)}(t,t_d)$ induced in the probe transition heterodyned with the probe pulse[63]

$$I_{pp}^{cat}(t_d) = \int_{\infty}^{-\infty}(|E_{probe}(t - t_d) + iP^{(3)}(t, t - t_d)|^2 - |E_{probe}(t - t_d)|^2)\, dt$$

$$= 2\,\mathrm{Im}\int_{\infty}^{-\infty}|E_{probe}(t - t_d)P^{(3)}(t, t - t_d)\, dt \qquad (7)$$

The sequential part of the signal $I_{pp,seq}^{cat}(t_d)$ can be correlated with the polarization $\rho_{34}(t)$ obtained from eqs 2−6

$$I_{pp,\,seq}^{cat}(t_d) \propto \mathrm{Im}\int_{\infty}^{-\infty} E_{probe}(t - t_d)\rho_{34}(t, t - t_d)\, dt \qquad (8)$$

Now we are set to take a look at the effect of the coherences on the pump−probe signals. Figure 5 shows results of the OBE signal according to eq 8 (data points), where the time constants for electron injection τ_{inj} and recombination τ_{rec} were chosen to be 15 fs and 1 ps, respectively. Three different situations are compared: no coherence ($T_2^{(1)*} = T_2^{(2)*} \rightarrow 0$) (squares), an intermediate situation with $T_2^{(1)*} = 15$ fs and $T_2^{(2)*} = 25$ fs (circles), and no pure dephasing ($T_2^{(1)*} = T_2^{(2)*} \rightarrow \infty$) (diamonds). The resulting total dephasing times $T_2^{(1)}$ for the neutral molecule are thus $\overset{\text{limit}}{\rightarrow}$ 0, 10, and 30 fs, respectively. Although the pure dephasing times $T_2^{(1)*}$ and $T_2^{(2)*}$ are unknown for the investigated system,[64] the intermediate parameter choice appears to be realistic for the experimental situation. Pump and probe fields are both considered as Gaussians of 28.3 fs fwhm, corresponding to a pulse duration of 20 fs. As expected, the OBE becomes exactly equivalent to the rate equation model in the limit of zero coherence. The significant effect of a finite dephasing time is a temporal shift of $I_{pp,seq}^{cat}(t_d)$ rather than changes in the shape of the signal (Figure 5). This shift arises from the fact that the rate of excitation reaches its maximum value a few femtoseconds after the maximum of the driving field[65] and can be as much as 11 fs for the given parameters. On the basis of changes in the shape of the signal, the time-dependent signals obtained with the OBEs were fitted with the rate equation model (eq 1 convoluted with a Gaussian system function of 28.3 fs fwhm). The fit requires that time zero, i.e., the temporal position of the maximum of the system function, is allowed as a free fit parameter. Under this condition the rate equation model reproduces the OBE signal quite reasonably; the best fits are given as solid lines in Figure 5. The injection times obtained from the fits are 16.6 fs for the intermediate situation and 17.8 fs for the limit $T_2^* \rightarrow \infty$. The latter case represents the upper limit for the deviation between OBE and rate equation results. For the intermediate situation the rate equation model overestimates the injection time by approximately 10%. However, if time zero is kept fixed at the position determined by the cross-correlation measurement, then the rate equation model may overestimate the injection time by up to 60%. Within this fit mode the failure of the rate equation model will depend on the method used for determining the cross-correlation. If the nonlinear signal is based on *nonresonant* transitions, which is usually the case, then the measured cross-correlation maps the true time zero of pump and probe pulses,[65] and the error of the fit reaches the maximum possible value. If *resonant* transitions are utilized, for instance, the rise of the excited-state absorption of a suitable dye, then the time shift between the OBE and the rate equation model is at least partially incorporated in the determined time zero. The error introduced by using the rate equation model for data fitting will be smaller in this situation.

The above comparison of the Bloch and the rate equation model suggests that the latter model is sufficient if time zero is allowed to be a free fit parameter. As the rate equation model contains only the minimal set of fit parameters, it results in very robust fits of the data and is therefore used for data fitting in this work. In principle, the temporal shift of the signal with respect to the true time zero could be utilized to gather information on the dephasing time. This has been pointed out recently within more advanced theoretical descriptions of pump−probe signals.[66,67] But this requires a very reliable determination of time zero measured at the sample position, i.e., in our case inside the UHV chamber. Cross-correlation measurements outside the chamber might not be accurate enough. For instance, the difference due to the dispersion in air outside the chamber compared to the dispersion-free path from the UHV window to the sample shifts time zero in the given experimental setup already by approximately 5 fs.

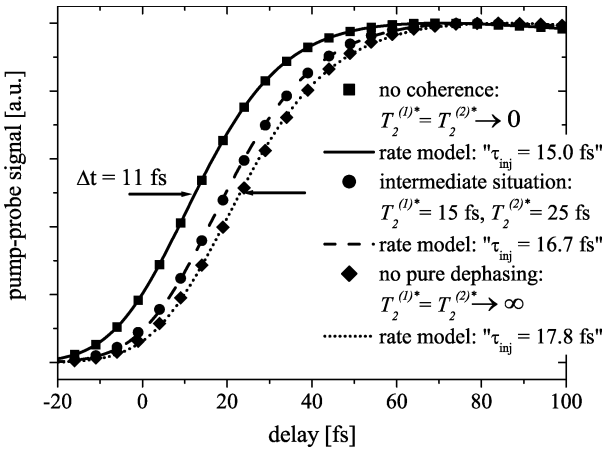

Figure 5. Simulated pump−probe signals $I_{pp,seq}^{cat}(t_d)$ for different dephasing: no coherence ($T_2^{(1)*} \rightarrow 0$, squares), no dephasing ($T_2^{(1)*} \rightarrow \infty$, diamonds), and an intermediate situation (circles, see legend and text). The solid, dashed, and dotted lines indicate least-squares fits of the simulated signal with the rate equation model.

Nonresonant transitions were excluded from the OBE solved here. The correct description of optical transitions pumped by spectrally broad pulses requires the consideration of the detuning between the field and the transition energy and the integration of the pulse spectrum.[62] However, incorporating a nonresonance term to the OBE acts equivalent to an additional dephasing term. The time shift between the rate equation model and the OBE would therefore be smaller when considering the detuning.[62,65] Another simplification of the OBE defined in eqs 2−6 is that only electronic states are incorporated; nuclear degrees of freedom are neglected. When considering vibronic states, pump and probe pulses might also generate vibrational coherence between two vibrational levels of one electronic state (ground or excited state), which might cause stimulated Raman scattering contributions to the pump−probe signal.[67] These contributions have the opposite sign of an absorption signal, which is not observed in the experiment. It should be noted that the calculated signal $I_{pp,seq}^{cat}(t_d)$ and the discussion above are explicitly addressing a pump−probe experiment with the cationic absorption as the probe transition. The temporal shifts induced by a finite dephasing will depend on the chosen transition. This should be taken into account, especially if ultrashort time constants are extracted employing a rate equation model to fit transient differences of several different electronic transitions.

The effect of dephasing on the pump−probe signal was discussed above with the constraint to only sequential contributions; i.e., the system interacts twice with the pump field and subsequently with the probe. However, the ordering of the interactions of the system with the fields may be mixed for

temporal overlap of pump and probe pulses, which gives rise to coherent contributions,[68−70] the so-called "coherent artifact".[71,72] These nonresonant effects superimpose and eventually mask the early sequential pump−probe signal. Nonresonant electronic coherences arising from the glass substrate or the unsensitized TiO_2 film were reduced here to below 10^{-4} transmission change by use of thin samples on thin glass substrates. The absence of a solvent is a great advantage in that context, as this usually is the main source of coherent contributions. Stimulated Raman scattering might also contribute with mixed field order, but as for the sequential term this effect is significant only for pump and probe pulses that are spectrally nearby. Finally, multiphoton absorption pathways should be considered. Multiphoton excitation of perylene has been investigated in several studies (see ref 73 and references therein). The existence of an S_n state between 37 000 and 38 000 cm^{-1} above S_0 accessible via two-photon absorption has been reported by different authors. The next higher state is assumed to be at approximately 45 000 cm^{-1}. The sum of the energies of the pump (435 nm) and probe (570 nm) pulses was approximately 40 500 cm^{-1}. Thus, incidentally this combination of pump and probe wavelengths does not match a possible two-photon transition. Therefore, multiphoton excitations did not contribute to the pump−(cation)−probe signals.

Within the time window considered in Figure 3, the recombination reaction, i.e., the reduction of the perylene cations by electron back-transfer from the semiconductor, does not appreciably set in, which allows monoexponential description of the dynamics. On longer time scales the recombination dynamics strongly deviates from a monoexponential behavior; even in the short time window of the first picosecond two exponentials are needed to fit the data of the DTB−Pe−COOH−TiO_2 system. This will be discussed in more detail in a future publication.

IV. Discussion

The following conclusions can be drawn from the data presented in the preceding sections. UPS and XPS measurements revealed that the energy of the photoexcited state of perylene is located in both the adsorbed dyes approximately 750 meV above the conduction band minimum; i.e., both perylene/anatase systems are in the wide band limit. In this situation all the Franck−Condon factors of the ET reaction are realized in parallel. Therefore the electronic coupling alone should control the electron injection time in this system rather than the Franck−Condon factors.[4,8,74] Thus, the strength of the electronic coupling of the perylene chromophore to the semiconductor can be estimated from the measured electron-transfer times to be a factor of 2 stronger with the carboxylic group than that with the phosphonic acid group as the anchor.[75] The linear absorption spectra of both dyes support this estimation qualitatively. Changes in the absorption spectra upon adsorption of the dyes on the surface can in principle arise from different effects. The most obvious one is the electronic interaction of the photoexcited state with semiconductor acceptor states resulting in a lifetime shortening and thus broadening of the absorption spectra. A change in the displacement between ground- and excited-state potential energy surfaces as well as a shift in the 0−0 transition energy can also occur for the adsorbed dye. Recently, Wang et al.[38] have analyzed the influence of different parameters on the change in the absorption spectra measured upon adsorption of the dyes on TiO_2 as shown in Figure 2. A fit to the experimental spectra revealed essentially that lifetime shortening with the same electron-transfer time for all the vibrational states was the dominant factor. At this point we want summarize with the qualitative conclusion that the absorption spectra indicate a significantly stronger electronic interaction of the perylene chromophore with TiO_2 when mediated by the carboxylic group compared to the phosphonic acid group. Significant differences in the geometries of the adsorbates and of the chemical nature of the anchor groups are the intuitive possible effects, which might cause this difference in electronic coupling strength.

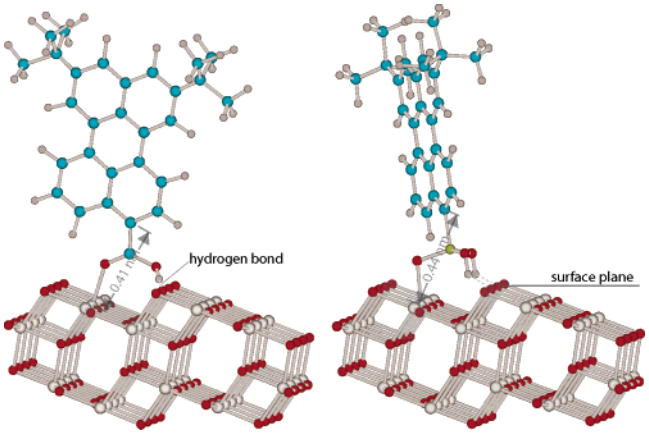

Figure 6. Geometries of monodentate adsorbed DTB−Pe−COOH (left) and DTB−Pe−PO_3H_2 (right) on a $Ti_{40}O_{80}$ anatase cluster with the (101) surface. See the text for details.

The binding configuration of the carboxylic group on nanostructured anatase has been investigated for several adsorbates, and as a conclusion the bidentate bridging coordination has been favored.[76−78] In agreement with these findings, Fourier transform infrared measurements of DTB−Pe−COOH show a quenching of the C═O stretching vibration at approximately 1680 cm^{-1} upon adsorption. Two binding configurations appear as the most likely ones if one considers the seven possible binding configurations discussed by Vittadini et al.[79] The calculated binding energies and the disappearance of the C═O band are compatible with the dissociative bidentate bridging configuration and a molecular adsorption with hydrogen bonding (see ref 79 for illustrations). Due to the hydrogen bond between the anchor and the surface, the latter configuration can be considered as a sort of bidentate binding as well.[79]

The potential tridentate binding of the phosphonate group gives rise to an even larger number of bonding possibilities. On the basis of IR and NMR spectroscopy studies, Guerrero and co-workers proposed the tridentate bonding to be the most likely adsorption mode on colloidal anatase, together with a bidentade configuration, which has a bridging geometry with a remaining OH group at the phosphorus.[80] Recently, Nilsing et al. studied the adsorption of phosphonic acid on the anatase (101) surface theoretically.[39] These authors found seven molecular as well as singly deprotonated dissociative adsorption geometries with similar binding energies above 40 kcal/mol. A truly tridentate binding of a doubly deprotonated phosphonate group seems to be unstable due to geometrical mismatch.[39] However, all stable molecular and singly deprotonated dissociative adsorption modes show three bonds as all hydroxyl groups form hydrogen bonds with surface oxygen atoms. These hydrogen bonds result in a tilt of the P−H bond away from the surface normal and thus of the long axis of perylene in a rigid adsorption geometry. This tilt is rather small with respect to the surface normal to the (101) surface of anatase,[39] i.e., the case considered in this paper, but becomes 58° from the surface normal on the rutile (110) face.[34]

Figure 6 depicts the molecular structures of DTB−Pe−COOH and DTB−Pe−PO_3H_2 at the anatase (101) surface. The most

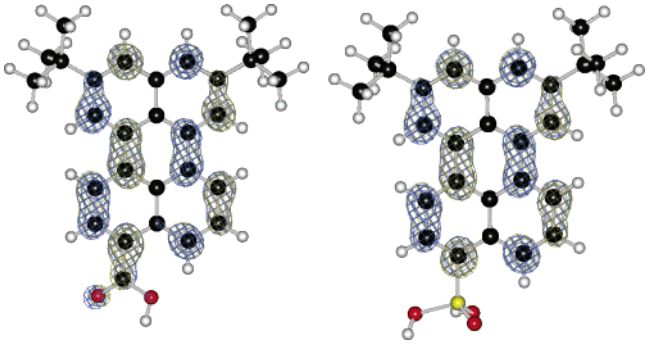

Figure 7. LUMO of isolated DTB−Pe−COOH (left) and DTB−Pe−PO_3H_2 (right).

stable adsorption geometries of formic and phosphonic acid according to ref 39 were chosen as the adsorption geometries. The molecular structures were obtained from a molecular mechanics (MM) cluster calculation with MM+ force field; the geometry of the cluster was frozen at the bulk structure. The distances between the chromophores and the surface, defined as the distance between the perylene carbon atom bound to the anchor group and the Ti surface atom binding to the anchor group are approximately 4.1 and 4.4 Å for the carboxylic and the phosphonic acid groups, respectively. The comparison of the alternative binding modes for both dyes provides a similar picture; i.e., the adsorbate−surface distance tends to be 5−10% larger in case of the phosphonic acid anchor compared to that of the carboxylic group. Although the applied computational method is rather basic and has limited accuracy, we exclude significant differences in the distance of the perylene ring structure from the surface for the two different anchor groups. Therefore the observed difference in the electron injection times by a factor of 2 is not considered a geometrical effect.

Figure 7 shows the LUMO wave functions of the isolated dyes as obtained from a semiempirical calculation. With respect to the eigenvectors, these states can be assumed to be a very good approximation of the excited-state wave functions since the electronic transition is an almost pure HOMO−LUMO transition.[49] The LUMOs have strong π^* character and are delocalized over the whole perylene backbone. The extension of the LUMOs onto the anchor group is significantly different for the two dyes, which can be explained by the different hybridization of both anchor groups: The sp^2-hybridized LUMO mixes more strongly with the sp^2-hybridized carboxylic group compared to the sp^3-hybridized phosphonate group. The partial charge density of the LUMOs shown in Figure 7 is approximately a factor of 10 larger on the −COOH group compared to that on the $-PO_3H_2$ group. However, it is important to note that these different spatial extensions do not affect significantly the absorption spectra of the isolated dyes in solution (Figure 2). The extension onto the anchor group is considered here a prerequisite for strong electronic interaction through the anchor group in the presence of a continuum of acceptor states. Recent DFT calculations of perylene dyes in the gas-phase and cluster calculations for the same dyes adsorbed on TiO_2 have confirmed the same qualitative interpretation of electron-transfer times linked to the spatial extension of the perylene donor orbital[40] as is suggested here based on semiempirical calculations. The influence of the anchor group reported here for the perylene dyes should be similar for other photosensitizers with an sp^2-hybridized photoexcited state, e.g., metal−organic dyes with polypyridyl ligands.

It is interesting to compare the adsorption energies of both anchor groups. Nilsing et al. have performed this comparison and have calculated a 60% higher adsorption energy of the most stable phosphonic acid adsorption geometry compared to that of formic acid.[39] This result is supported by the experimental observation that carboxyalkylphosphonic bi-acids form self-assembled monolayers on colloidal TiO_2 with the phosphonic acid binding to the surface rather than the carboxylic group.[81,82] Therefore, the phosphonic acid group appears for most applications as the preferable anchor because of its stronger binding to the surface of TiO_2 compared to the carboxylic group. It is shown in this paper that electronic coupling through the phosphonic acid group is still strong enough to facilitate photoinduced electron transfer on the time scale of a few tens of femtoseconds, i.e., 28 fs in the case of the chromophore perylene.

V. Summary

The influence of the anchor group on the dynamics of HET was studied for the perylene−anatase system. The chromophore was linked via either a carboxylic or a phosphonic acid to the semiconductor. The energetic positions of the photoexcited donor states of the ET reactions were found to be approximately 750 meV above the CBM for both these dyes. Under this condition, differences in the kinetics of the ET mainly arise from differences in the strength of the electronic coupling between the adsorbate and the semiconductor. Pump−probe spectroscopy revealed electron injection time constants of 13 and 28 fs for perylene bound via the carboxylic and phosphonic acid, respectively. The validity of applying a simple rate equation model for the extraction of time constants in this time scale was verified by comparing the rate equation model with an optical Bloch equation model. The comparison of the changes in the dye absorbance upon adsorption support the conclusion that the electronic coupling mediated by the carboxylic group is significantly higher compared to the phosphonic one. This effect most likely arises from differences in the local symmetry of the anchor groups rather than differences in the adsorbate−surface distance.

Acknowledgment. Financial support by the German Science Foundation through SFB 450 (R.E.) and SPP 1093 (L.G.) is gratefully acknowledged. We are grateful to P. Persson and V. May for helpful discussions. We appreciate the preparation of the nanoporous TiO_2 electrodes by U. Michalczik and are grateful to S. Kubala for excellent technical support with the UPS measurements. We are grateful to S. Imme (elemental analyses) as well as M. Dettlaff and H.-J. Kroth (NMR measurements) from the Technical University Berlin.

Supporting Information Available: Description of the syntheses of the perylene dyes. This material is available free of charge via the Internet at http://pubs.acs.org.

References and Notes

(1) Sturmer, D. M.; Heseltine, D. W. In *The Theory of the Photographic Process*; James T. H., Ed.; MacMilian Publishing: New York, 1977.
(2) O'Regan, B.; Grätzel, M. *Nature (London)* **1991**, *353*, 737.
(3) *Molecular Electronics*; Jortner, J., Ratner, M. A., Eds.; Blackwell Science: Oxford, U. K., 1997.
(4) Ramakrishna, S.; Willig, F.; May, V. *Phys. Rev. B* **2000**, *62*, R16330.
(5) Wang, L.; Willig, F.; May, V. *J. Chem. Phys.* **2006**, *124*, 014712.
(6) Ramakrishna, S.; Willig, F.; May, V.; Knorr, A. *J. Phys. Chem. B* **2003**, *107*, 607.
(7) Lanzafame, J. M.; Miller, R. J. D.; Muenter, A. A.; Parkinsons, B. A. *J. Phys. Chem.* **1992**, *96*, 2820.
(8) Miller, R. J. D.; McLendon, G.; Nozik, A.; Schmickler, W.; Willig, F. *Surface Electron-Transfer Processes*; VCH Publishers: New York, 1995.

(9) Willig, F.; Zimmermann, C.; Ramakrishna, S.; Storck, W. *Electrochim. Acta* **2000**, *45*, 4565.
(10) Burfeindt, B.; Hannappel, T.; Storck, W.; Willig, F. *J. Phys. Chem.* **1996**, *100*, 16463.
(11) Huber, R.; Moser, J.-E.; Grätzel, M.; Wachtveitl, J. *J. Phys. Chem. B* **2002**, *106*, 6494.
(12) Eichberger, R.; Willig, F. *Chem. Phys.* **1990**, *141*, 159.
(13) Benkö, G.; Kallioinen, J.; Korpi-Tommola, J.; Yartsev, A.; Sundström, V. *J. Am. Chem. Soc.* **2002**, *124*, 489.
(14) Schnadt, J.; Brühwiler, B.; L. Patthey.; O'Shea, J.; Södergren, S.; Odelius, M.; Ahuja, R.; Karis, O.; Baessler, M.; Persson, P.; Siegbahn, H.; Lunell, S.; Martensson, N. *Nature (London)* **2002**, *418*, 620.
(15) Anderson, N. A.; Ai, X.; Lian, T. *J. Phys. Chem. B* **2003**, *107*, 14414.
(16) Tachibana, Y.; Moser, J. E.; Grätzel, M.; Klug, D. R.; Durrant, J. R. *J. Phys. Chem. B* **1996**, *100*, 20056.
(17) Hannappel, T.; Burfeindt, B.; Storck, W.; Willig, F. *J. Phys. Chem. B* **1997**, *101*, 6799.
(18) Wang, Y.; Asbury, J. B.; Lian, T. *J. Phys. Chem. A* **2000**, *104*, 4291.
(19) Pelet, S.; Grätzel, M.; Moser, J. E. *J. Phys. Chem. B* **2003**, *107*, 3215.
(20) Kallioinen, J.; Benkö, G.; Sundström, V.; Korppi-Tommola, J. E. I.; Yartsev, A. P. *J. Phys. Chem. B* **2002**, *106*, 4396.
(21) Bauer, C.; Boschloo, G.; Mukhtar, E.; Hagfeldt, A. *J. Phys. Chem. B* **2001**, *105*, 5585.
(22) Duncan, W. R.; Stier, W. M.; Prezhdo, O. V. *J. Am. Chem. Soc.* **2005**, *127*, 7941.
(23) Abuabara, S. G.; Rego, L. G. C.; Batista, V. S. *J. Am. Chem. Soc.* **2005**, *127*, 18234.
(24) Töben, L.; Gundlach, L.; Ernstorfer, R.; Eichberger, R.; Hannappel, T.; Willig, F.; Zeiser, A.; Förstner, J.; Knorr, A.; Hahn, P. H.; Schmidt, W. G. *Phys. Rev. Lett.* **2005**, *94*, 067601.
(25) Moser, J.; Punchihewa, S.; Infelta, P. P.; Grätzel, M. *Langmuir* **1991**, *7*, 3012.
(26) Duncan, W. R.; Prezhdo, O. V. *J. Phys. Chem. B* **2005**, *109*, 365.
(27) Persson, P.; Bergström, R.; Lunell, S. *J. Phys. Chem. B* **2000**, *104*, 10348.
(28) Gundlach, L.; Ernstorfer, R.; Willig, F. *Phys. Rev. B* **2006**, *74*, 035324.
(29) Trösken, B.; Willig, F.; Schwarzburg, K.; Ehert, A.; Spitler, M. *J. Phys. Chem.* **1995**, *99*, 5152.
(30) Ernstorfer, R.; Felber, S.; Storck, W.; Galoppini, E.; Wei, Q.; Willig, F. *Res. Chem. Intermed.* **2005**, *31*, 643.
(31) Vrachnou, E.; Vlachopoulos, N.; Grätzel, M. *J. Chem. Soc., Chem. Commun.* **1987**, 868.
(32) Blackbourn, R. L.; Johnson, C. S.; Hupp, J. T. *J. Am. Chem. Soc.* **1991**, *113*, 1060.
(33) Fujihira, M.; Ohishi, N.; Ota, T. *Nature (London)* **1977**, *268*, 226.
(34) Gundlach, L. Ph.D. Thesis, Freie Universität Berlin, Berlin, 2005.
(35) Shklover, V.; Nazeeruddin, M.-K.; Zakeeruddin, S. M.; Barbe, C.; Kay, A.; Haibach, T.; Steurer, W.; Hermann, R.; Nissen, H.-U.; Grätzel, M. *Chem. Mater.* **1997**, *9*, 430.
(36) Burfeindt, B.; Zimmermann, C.; Ramakrishna, S.; Hannappel, T.; Meiβner, B.; Storck, W.; Willig, F. *Z. Phys. Chem.* **1999**, *212*, 67.
(37) Yeh, A. T.; Shank, C. V.; McCusker, J. K. *Science* **2000**, *289*, 935.
(38) Wang, L.; Ernstorfer, R.; Willig, F.; May, V. *J. Phys. Chem. B* **2005**, *109*, 9589.
(39) Nilsing, M.; Lunell, S.; Persson, P.; Ojamäe, L. *Surf. Sci.* **2005**, *582*, 49.
(40) Persson, P.; Lundqvist, M. J.; Ernstorfer, R.; Goddard, W. A., III.; Willig, F. *J. Chem. Theory Comput.* **2006**, *2*, 441.
(41) Nazeeruddin, M.-K.; Kay, A.; Rodicio, I.; Humphry-Baker, R.; Muller, E.; Liska, P.; Vlachopoulus, N.; Grätzel, M. *J. Am. Chem. Soc.* **1993**, *115*, 6382.
(42) Zimmermann, C.; Willig, F.; Ramakrishna, S.; Burfeindt, B.; Pettinger, B.; Eichberger, R.; Storck, W. *J. Phys. Chem. B* **2001**, *105*, 9245.
(43) Ernstorfer, R. Ph.D. Thesis, Freie Universität Berlin, Berlin, 2004.
(44) Ristagno, C. V.; Shine, H. J. *J. Org. Chem.* **1971**, *36*, 4050.
(45) Dittrich, T.; Weidmann, J.; Koch, F.; Uhlendorf, I.; Lauermann, I. *Appl. Phys. Lett.* **1999**, *75*, 3980.
(46) Wilhelm, T.; Piel, J.; Riedle, E. *Opt. Lett.* **1997**, *22*, 1494.
(47) Gundlach, L.; Ernstorfer, R.; Riedle, E.; Eichberger, R.; Willig, F. *Appl. Phys. B: Laser Opt.* **2005**, *80*, 727.
(48) Piel, J.; Riedle, E.; Gundlach, L.; Ernstorfer, R.; Eichberger, R. *Opt. Lett.* **2006**, *31*, 1289.
(49) Halasinski, T. M.; Weisman, J. L.; Ruiterkamp, R.; Lee, T. J.; Salama, F.; Head-Gordon, M. *J. Phys. Chem. A* **2003**, *107*, 3660.
(50) Lochbrunner, S.; Huppmann, P.; Riedle, E. *Opt. Commun.* **2000**, *184*, 321.
(51) Asahi, R.; Taga, Y.; Mannstadt, W.; Freeman, A. J. *Phys. Rev. B* **2000**, *61*, 7459.
(52) Sanjines, R.; Tang, H.; Berger, H.; Gozzo, F.; Margaritondo, G.; Levy, F. *J. Appl. Phys.* **1994**, *75*, 2945.
(53) Thomas, A. G.; Flavell, W. R.; Kumarasinghe, A. R.; Mallik, A. K.; Tsoutsou, D.; Smith, C. G.; Stockbauer, R.; Patel, S.; Grätzel, M.; Hengerer, R. *Phys. Rev. B* **2003**, *67*, 035110.
(54) Mott, N. F.; Davis, E. A. *Electronic Processes in Non-Crystalline Materials*; Clarendon Press: Oxford, U. K., 1979.
(55) Boschi, R.; Murrell, J. N.; Schmidt, W. *Faraday Discuss. Chem. Soc.* **1972**, *54*, 116.
(56) Ishii, H.; Sugiyama, K.; Ito, E.; Seki, K. *Adv. Mater.* **1999**, *11*, 605.
(57) Schlaf, R.; Schroeder, P. G.; Nelson, M. W.; Parkinson, B. A.; Lee, P. A.; Nebesny, K. W.; Armstrong, N. R. *J. Appl. Phys.* **1999**, *86*, 1499.
(58) Westermark, K.; Henningsson, A.; Rensmo, H.; Södergren, S.; Siegbahn, H.; Hagfeldt, A. *Chem. Phys.* **2002**, *285*, 157.
(59) Joblin, C.; Salama, F.; Allamandola, L. *J. Chem. Phys.* **1999**, *110*, 7287.
(60) Joblin, C.; Salama, F.; Allamandola, L. *J. Chem. Phys.* **1995**, *102*, 9743.
(61) Stier, W.; Prezhdo, O. V. *J. Mol. Struct. (THEOCHEM)* **2003**, *630*, 33.
(62) Loudon, R. *The Quantum Theory of Light*; Oxford University Press: New York, 1983.
(63) Mukamel, S. *Principles of Nonlinear Optical Spectroscopy*; Oxford University Press: New York, 1995.
(64) Femtosecond two-photon photoemission data for the same chromophores on the surface of a TiO_2 single crystal analyzed with an OBE model indicate a very fast dephasing with time constants below the ET time constants.[34]
(65) Hertel, T.; Knoesel, E.; Wolf, M.; Ertl, G. *Phys. Rev. Lett.* **1996**, *76*, 535.
(66) Farrow, D. A.; Yu, A.; Jonas, D. M. *J. Chem. Phys.* **2003**, *118*, 9348.
(67) Dobryakov, A. L.; Kovalenko, S. A.; Ernsting, N. P. *J. Chem. Phys.* **2003**, *119*, 988.
(68) Boyd, R. W.; Mukamel, S. *Phys. Rev. A* **1984**, *29*, 1973.
(69) Che, J.; Zhang, W.; Yan, Y. *J. Chem. Phys.* **1997**, *106*, 6947.
(70) Kovalenko, S. A.; Dobryakov, A. L.; Ruthmann, J.; Ernsting, N. P. *Phys. Rev. A* **1999**, *59*, 2369.
(71) Ekvall, K.; van der Meulen, P.; Dhollande, C.; Berg, L.-E.; Pommeret, S.; Naskrecki, R.; Mialocq, J.-C. *J. Appl. Phys.* **2000**, *87*, 2340.
(72) Lorenc, M.; Ziolek, M.; Naskrecki, R.; Karolczak, J.; Kubicki, J.; Maciejewski, A. *Appl. Phys. B: Laser Opt.* **2002**, *74*, 19.
(73) Greever, J. S.; Turner, J. B. M.; Kauffman, J. F. *J. Phys. Chem. B* **2003**, *107*, 4072.
(74) Ramakrishna, S.; Willig, F. *J. Phys. Chem. B* **2000**, *104*, 68.
(75) Muscat, J. P.; Newns, D. M. *Prog. Surf. Sci.* **1978**, *9*, 1.
(76) Duffy, N. W.; Dobson, K. D.; Gordon, K. C.; Robinson, B. H.; McQuillan, A. J. *Chem. Phys. Lett.* **1997**, *266*, 451.
(77) Finnie, K. S.; Bartlett, J. R.; Woolfrey, J. L. *Langmuir* **1998**, *14*, 2744.
(78) Bauer, C.; Boschloo, G.; Mukhtar, E.; Hagfeldt, A. *J. Phys. Chem. B* **2002**, *106*, 12693.
(79) Vittadini, A.; Selloni, A.; Rotzinger, F. P.; Grätzel, M. *J. Phys. Chem. B* **2000**, *104*, 1300.
(80) Guerrero, G.; Mutin, P. H.; Vioux, A. *Chem. Mater.* **2001**, *13*, 4367.
(81) Pawsey, S.; Yach, K.; Reven, L. *Langmuir* **2002**, *18*, 5205.
(82) Pawsey, S.; McCormick, M.; Paul, S. D.; Graf, R.; Lee, Y. S.; Reven, L.; Spiess, H. W. *J. Am. Chem. Soc.* **2003**, *125*, 4174.-